

Supporting Information

How Strain Affects the Reactivity of Surface Metal Oxides

Kazuhiko Amakawa, Lili Sun, Chunsheng Guo, Michael Hävecker, Pierre Kube, Israel E. Wachs, Soe Lwin,

*Anatoly I. Frenkel, Anitha Patlolla, Klaus Hermann, Robert Schlögl and Annette Trunschke**

*trunschke@fhi-berlin.mpg.de

Content

1. Complete Reference for [3] and [25]
2. Experimental and Theoretical Methods
3. Extended Characterization of MoO_x/SBA-15
4. Selectivity Data in Oxidative Dehydrogenation of Propane over MoO_x/SBA-15

1. Complete Reference for [3] and [25]

[3] Behrens, M.; Studt, F.; Kasatkin, I.; Kühl, S.; Hävecker, M.; Abild-Pedersen, F.; Zander, S.; Girgsdies, F.; Kurr, P.; Knief, B.-L.; Tovar, M.; Fischer, R. W.; Nørskov, J. K.; Schlögl, R. *Science* **2012**, 336, 893–897.

[25] Vojvodic, A.; Calle-Vallejo, F.; Guo, W.; Wang, S.; Toftelund, A.; Studt, F.; Martínez, J. I.; Shen, J.; Man, I. C.; Rossmeisl, J.; Bligaard, T.; Nørskov, J. K.; Abild-Pedersen, F. *J. Chem. Phys.* **2011**, 134, 244509–244509–8.

2. Experimental and Theoretical Methods

2.1. Preparation of Supported MoO_x/SBA-15

To obtain highly dispersed molybdenum oxide species on mesoporous silica SBA-15, an anion exchange procedure was employed.^[1] The preparation details have been described elsewhere.^[2] In brief, freshly synthesized metal-free SBA-15 (internal sample ID 8233) was functionalized with propylammonium chloride using (3-aminopropyl)trimethoxysilane followed by treatment with hydrochloric acid. Then, the functionalized SBA-15 powder was stirred in an aqueous solution containing the desired amount of ammonium heptamolybdate to perform anion exchange. After washing with water and filtration, the material was dried and calcined at 823 K in air, yielding supported MoO_x/SBA-15 with the actual loadings of 2.1, 5.1, 6.6, 8.2 and 13.3 Mo% (internal sample ID 8442, 8440, 11054, 11055 and 8441, respectively). The sample labels are given in Table S2.

2.2. General Characterization

Nitrogen adsorption was carried out at 77 K on a Quantachrome Autosorb-6B analyzer. Prior to the measurement, the samples were outgassed in vacuum at 393 K for 16 h. The data were processed on Autosorb software (Quantachrome). The specific surface area A_s was calculated according to the multipoint Brunauer-Emmett-Teller method (BET) in the pressure range $p/p_0 = 0.05-0.15$ assuming a N₂ cross sectional area of 16.2 Å². The micropore surface area A_μ and micropore volume V_μ were estimated using the t -plot method in the statistical thickness $t = 4.5-6.5$ Å range. The total pore volume V_p was estimated by using the amount of physisorbed nitrogen at a relative pressure $P/P_0 = 0.95$. The pore size distribution was determined by NLDFT method using a model based on equilibrated adsorption of N₂ on silica assuming cylindrical pores at 77 K.

For chemical analysis, the samples and corresponding MoO₃ standards were mixed with lithiumtetraborate flux (FX-X100, Fluxana) and fused in a Vulcan Fusion Machine (HD Electronic & Elektrotechnik GmbH) under formation of flat molten glass discs, which were analyzed by X-Ray Fluorescence spectroscopy using the spectrometer Pioneer S4 (Bruker AXS GmbH).

Powder X-ray Diffraction (XRD) analysis was performed using a STOE STADI-P transmission diffractometer equipped with CuK_{α1} radiation.

The concentration of surface silanol groups of SBA-15 was determined by thermogravimetry (TG) using a Netzsch STA449 Jupiter thermoanalyzer. After the dehydration at 823 K for 1 h under argon stream, the temperature was raised with 10 K min⁻¹ to 1473 K and held for 0.5 h. The concentration of surface hydroxyl groups was calculated based on the mass loss between 823 K and 1473 K assuming that one water molecule is formed by condensation of two hydroxyl groups.^[3]

The morphology and local content of molybdenum was studied by scanning electron microscopy (SEM) coupled with energy-dispersive X-ray analysis (EDX) using a Hitachi S-4800 electron microscope operating at 2 kV in secondary electron (SE) mode and backscattering electron (BSE) mode.

2.3. Temperature-Programmed Reduction with Hydrogen (H₂-TPR)

Temperature-programmed reduction with hydrogen (H₂-TPR) was performed for supported MoO_x/SBA-15 in the dehydrated state using a quartz-made tubular gas flow reactor operating at atmospheric pressure. After the

pretreatment at 823 K (heating rate 10 K·min⁻¹) for 0.5 h in a dehydrated 20 % O₂ in Ar flow, consumption of hydrogen during heating in 2 % H₂ in argon (20 ml min⁻¹, 323 to 1253 K, heating rate 10 K min⁻¹) was monitored with a quadrupole mass spectrometer (QMS200, Balzer) using argon as internal standard. The sample weight was varied to keep the amount of molybdenum at about 50 μmol.

2.4. Spectroscopy

Prior to spectroscopic measurements, unless stated, the samples were calcined in dry oxygen (20 kPa, neat or diluted with a dry inert gas) at 823 K (heating rate 10 K·min⁻¹) for 0.5 h, then cooled to room temperatures in the presence of oxygen in order to achieve the fully oxidized and dehydrated state of the catalyst (referred to as “the dehydrated state”).

UV—vis. The UV-visible (UV—vis) diffuse reflectance spectra were taken at room temperature with a PerkinElmer Lambda 650 instrument equipped with an in situ cell (Harrick Praying Mantis™ diffuse reflectance attachment DRP-P72 in combination with a HVC-VUV reaction chamber). The dehydrated SBA-15 was used as the white standard. To assure good spectral quality, the maximum value of Kubelka-Munk function $F(R)$ was kept below 1 by diluting the sample with the SBA-15 white standard. The spectra were normalized at 4.51 eV.

Mo K-edge XAS. Mo K-edge X-ray absorption spectroscopy (XAS) was performed in transmission mode at the beam line X18B at the National Synchrotron Light Source (NSLS) at the Brookhaven National Laboratory, using ionization chamber detectors for measuring incident and transmitted beam intensities. In addition, a third ionization chamber was used to detect the beam through a reference Mo foil, for energy calibration and alignment purposes. A quartz capillary cell (I.D./O.D. = 0.8 / 1.0 mm) was used for in situ measurements. Data processing and analysis were performed using Athena and Artemis softwares.^[4]

O K-edge NEXAFS. In situ O K-edge near edge X-ray absorption fine structure spectroscopy (NEXAFS) was performed in the presence of 0.5 mbar O₂ at 623 K in the Auger electron yield mode at the synchrotron radiation facility BESSY II of the Helmholtz-Zentrum Berlin, Germany (HZB), using monochromatic radiation of the ISSS (Innovative Station for In Situ Spectroscopy) beamline as a tunable X-ray source. O K-edge spectra of the sample surface have been corrected for the remaining effects of O₂ gas phase absorption. Details of the setup, metrology and data treatment are presented elsewhere.^[5-7]

Raman. Confocal Raman spectra were collected at room temperature using a Horiba-Jobin Yvon LabRam instrument equipped with a red laser excitation (633 nm / 1.96 eV, 1.5 mW at the sample position) and a Horiba-Jobin Yvon LabRam HR instrument equipped with an UV laser excitation (325 nm / 3.82 eV, laser power of 5 mW at the sample position). Spectral resolutions were better than 2 cm⁻¹. In situ cells (a home-made quartz cell and a Linkam CCR1000) were used to measure the dehydrated state.

FTIR. Diffuse reflectance FT infrared (IR) spectra were collected at room temperature on a Bruker IFS66 spectrometer equipped with a liquid nitrogen-cooled MCT detector at a spectral resolution of 4 cm⁻¹ and accumulation of 1024 scans. An in situ cell (Harrick Praying Mantis™ diffuse reflectance attachment DRP-P72 in combination with a HVC-VUV reaction chamber) was used. KBr was used as reference material. The spectra were normalized using the silica band at 1865 cm⁻¹.

2.5. Theoretical Studies

Cluster Models. The silica-supported monomeric molybdena structures are modeled by polyhedral oligomeric silsesquioxane-based clusters.^[7] The model clusters **a—c** contain tetrahedral di-oxo (Si—O—)₂Mo(=O)₂ units. Figure S1 shows the optimized geometric structures of the clusters.

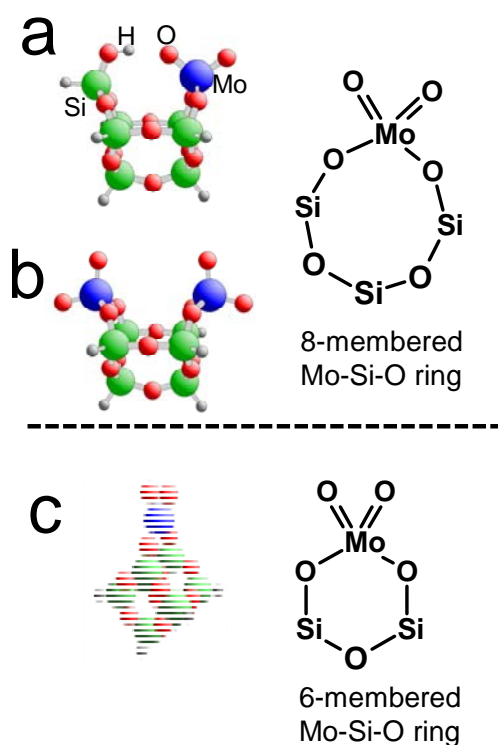


Figure S1. Geometric structure of the molybdena—silica model clusters having tetrahedral di-oxo units in a stick-ball representation: (a) $\text{MoO}_4\text{—Si}_7\text{O}_{10}\text{H}_8$, (b) $(\text{MoO}_4)_2\text{—Si}_6\text{O}_7\text{H}_6$, (c) $\text{MoO}_4\text{—Si}_8\text{O}_{12}\text{H}_6$

The tetrahedral MoO_4 units in cluster **a** and **b** are anchored on silica to form 8-membered Mo—Si—O rings, while cluster **c** comprises a 6-membered Mo—Si—O ring. The difference between **a** and **b** is that **a** represents a di-oxo structure in the neighborhood of a silanol species, and **b** models two adjacent Mo di-oxo species.

Table S1. Bond distances and angles in the Mo—Si—O clusters having tetrahedral di-oxo MoO_4 structures (Figure S1).

Cluster	distance (Å)			angle (°)
	Mo=O ^a	Mo—O ^b	Si—Si ^c	O=Mo=O ^a
a : $\text{MoO}_4\text{—Si}_7\text{O}_{10}\text{H}_8$	1.70—1.71	1.87	4.6	108.1
b : $(\text{MoO}_4)_2\text{—Si}_6\text{O}_7\text{H}_6$	1.70	1.89	4.7	107.7
c : $\text{MoO}_4\text{—Si}_8\text{O}_{12}\text{H}_6$	1.92—1.93	2.02	3.07	43.9

^a terminal molybdenum—oxygen bonds, ^b at the bridging Mo—O—Si bonds, ^c the Si atoms at the two bridging Mo—O—Si bonds.

Calculations of O K-edge NEXAFS and FTIR Spectra. Theoretical O 1s X-ray absorption spectra of the model clusters were calculated by density-functional theory (DFT) using the transition potential approach and applying the StoBe cluster code.^[8] Further details of NEXAFS spectra calculation are described elsewhere.^[7] Theoretical IR spectra of selected clusters were calculated by DFT at BLYP level using DZP basis set employing deMon2k software.^[9]

2.6. Catalytic Tests

Propane Metathesis The catalytic activity for the self metathesis of propene to ethene and 2-butenes was measured using a fixed-bed tube flow reactor at atmospheric pressure. All the gases were thoroughly dehydrated and deoxygenated (except oxygen) using trapping filters. The catalysts were pressed under ~ 135 MPa, crushed and sieved to a particle size of 250-355 μm . Then, 100 mg of the catalyst was loaded into a U-shaped quartz reactor with an inner diameter of 4 mm. Guard beds consisting of silica gel (BET surface area = 428 $\text{m}^2 \text{g}^{-1}$) were placed both immediately above (100 mg) and below (50 mg) the catalyst bed in order to protect the catalyst bed from possible contamination by water. The use of the silica guard beds is essential to obtain a good catalytic performance. A blank test using bare SBA-15 with silica beds confirmed inertness of the apparatus and the guard beds. The catalyst was activated at 823 K (heating rate 10 $\text{K} \cdot \text{min}^{-1}$) for 0.5 h, cooled to 323K in a 20 % O_2 in Ar (20 $\text{ml} \text{min}^{-1}$), and then flushed with a flow of Ar (20 $\text{ml} \text{min}^{-1}$) before reaction. A neat propene flow of 8 $\text{ml} \text{min}^{-1}$ was fed to start the reaction. Inlet and outlet gases were analyzed by on-line gas chromatography using an Agilent Technologies 6890A GC system equipped with a flame ionization detector. The conversion of propene was kept below 5 % to stay in a differential regime. The selectivity to the metathesis products (ethane, cis- and trans-butene) was above 99.5 %, while trace amounts of 1-butene and higher hydrocarbons were detected. The catalytic activity was measured at 15~21h of time on stream. The activity is presented as formation rate of the metathesis products (i.e. sum of ethane, cis- and trans-butene) normalized by specific surface area of the catalyst.

Oxidative Dehydrogenation of Propane The catalytic activity for oxidative dehydrogenation of propane was tested at 773 K applying a contact time of 0.6 $\text{g} \cdot \text{s} \cdot \text{ml}^{-1}$ (catalyst mass = 0.1g, total flow rate = 10 $\text{ml} \cdot \text{min}^{-1}$) and a molar ratio of propane : oxygen = 2 : 1 with nitrogen as balance ($\text{C}_3\text{H}_8/\text{O}_2/\text{N}_2=10/5/85$). The experiments were carried out in a setup equipped with 8 parallel fixed bed quartz reactors at atmospheric pressure. The catalysts were pressed under ~ 135 MPa, crushed and sieved to a particle size of 250-355 μm . Reactants and products were analyzed by an online gas chromatograph (Agilent 7890). Separation of the permanent gases CO , CO_2 , N_2 and O_2 was achieved with a combination of a Plot-Q and a Plot-molsieve column connected to a thermal conductivity detector (TCD). Propane and propylene, were separated with a Plot-Q column connected to a flame ionization detector (FID). Conversion of propane and selectivity to oxidation products were calculated based on the number of carbon atoms and on the sum of products found. The catalytic activity was measured at 13 days of time on stream. The activity is presented as consumption rate of propane normalized by specific surface area of the catalyst.

3. Extended Characterization of MoO_x/SBA-15

3.1. Texture and Dispersion

The N₂ physisorption shows that the cylindrical mesoporous structure of SBA-15 (~ 7nm) prevails after introduction of MoO_x, as can be seen in the characteristic type-IV isotherms with H1-type hysteresis patterns (Figure S2) and derived pore diameters (d_p , in Table S2). Surface area (A_s) and pore volume (V_p) are significantly decreased in the Mo containing catalysts (Table S2) largely due to preferential filling of the micropores in the course of Mo deposition (Table S2).

Table S2. Properties of MoO_x/SBA-15

sample name	Mo loading ^a (wt%)	Surface density		A_s (m ² /g)	A_μ ^e		V_p ^g (ml/g)	d_p ^h (nm)
		Mo ^b (nm ⁻²)	SiOH ^{c, d} (nm ⁻²)		(m ² /g)	(%) ^f		
SBA-15	0	0	1.6 ^c	859	261	36	1	7.5
2.1M	2.1	0.21	1.1 ^d	637	164	31	0.79	7.1
5.1Mo	5.1	0.58	0.88 ^d	554	127	28	0.71	7.1
6.6Mo	6.6	0.85	0.68 ^d	490	135	28	0.61	7.1
8.2Mo	8.2	1.13	0.51 ^d	457	147	31	0.58	7.0
13.3Mo	13.3	2.51	0.07 ^d	332	36	13	0.55	7.4

^a by XRF, ^b Mo loading (at%) divided by A_s , ^c by TG, ^d by IR at the dehydrated state using relative heights of the silanol peak at 3745 cm⁻¹, ^e micropore (< ~0.9 nm of width) surface estimated by t -plot method, ^f A_μ divided by A_s , ^g at $P/P_0 = 0.95$, ^h at the dehydrated state; ^h estimated by NLDFT approach.

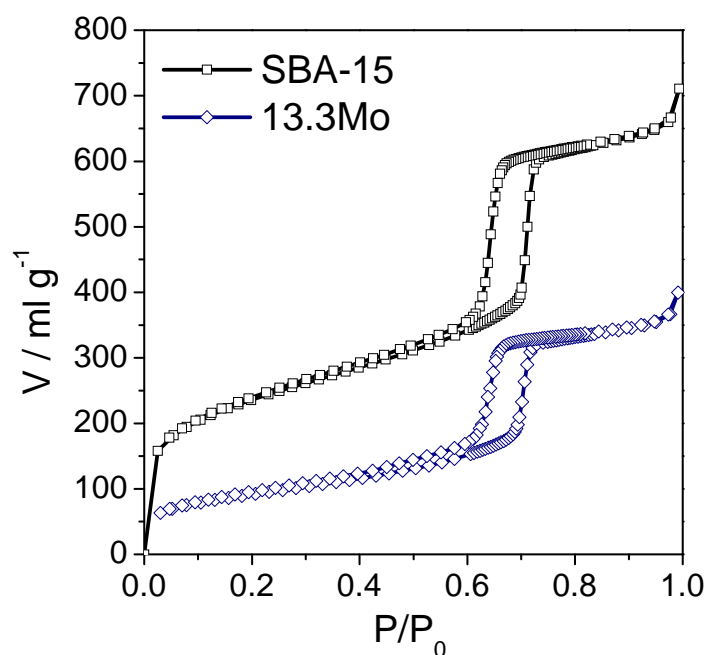


Figure S2. Selected adsorption/desorption isotherms of nitrogen on supported MoO_x/SBA-15 (13.3wt%_Mo) and SBA-15 measured at 77 K. Note that all the supported MoO_x/SBA-15 samples show similar Type-IV isotherms with H1 type hysteresis patterns at $P/P_0 = \sim 0.65$.

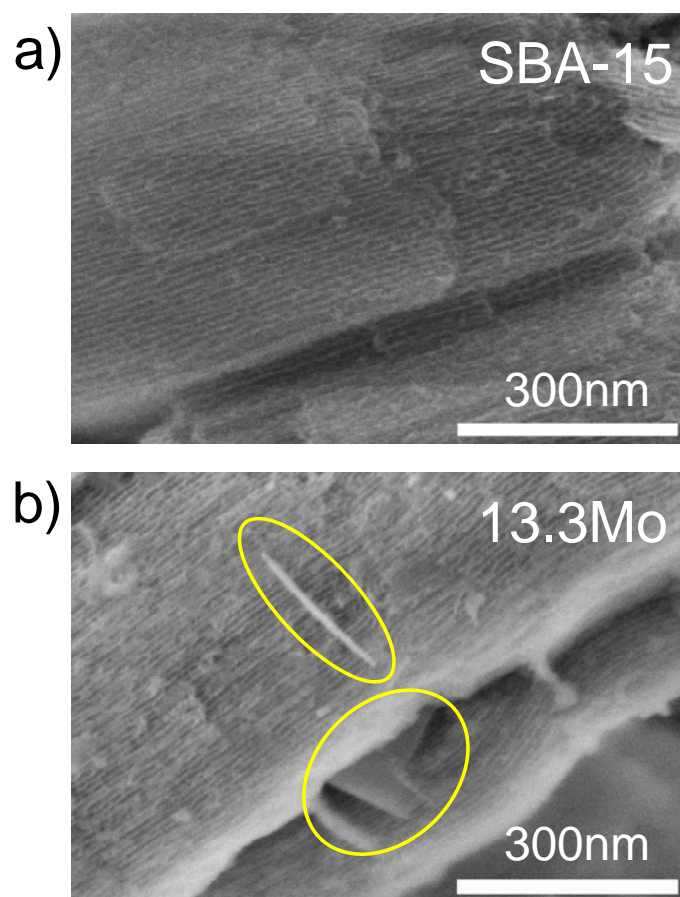


Figure S3. High resolution SEM images of SBA-15 (a) and 13.3Mo (b). Plate-like crystalline MoO₃ particles are highlighted by the yellow circles in (b).

SEM-EDX confirmed a homogeneous distribution of Mo (data not shown) except in case of the catalyst 13.3Mo. In 13.3Mo, a minor amount of plate-like particles was found in the SEM image (Figure S3b). These particles are identified as crystalline MoO₃ by the characteristic plate-like morphology, the local Mo content determined by EDX (ca. 60%; the theoretical content of MoO₃ is 67%), the occurrence of characteristic bands due to MoO₃ (e.g. 993, 817 and 665 cm⁻¹)^[10] in the Raman spectrum (Figure S6A) and by XRD that exhibits very weak MoO₃ reflection peaks (not shown). The regions free of crystalline MoO₃ possess a loading of 12.9±0.5 wt% Mo that is close to the overall content determined by XRF (13.3 wt%), which suggests that the vast majority (~97%, estimated by the comparison of XRF and EDX) of the supported molybdena is present as surface MoO_x species that are not detectable in the SEM images because of their non-crystalline nature. It is noted that the Raman spectrum of 13.3Mo (Figure S6A) shows intense bands due to crystalline MoO₃ (e.g. 993, 817 and 665 cm⁻¹)^[10] owing to the very high Raman scattering cross section of MoO₃.^[11,12] However, the corresponding IR spectrum does not show detectable features of MoO₃ as the relative concentration of this phase is very low as revealed by SEM-EDX. Neither Raman spectroscopy nor XRD show any sign of segregated MoO₃ nanoparticles in the Mo catalysts with loadings lower than 13.3% Mo.

3.2. Mo K-edge XAS

XANES The Mo K-edge X-ray absorption near-edge structure (XANES) spectra show a pronounced pre-edge peak at 20006 eV (Figure 2b) that is mainly due to the dipole transitions from Mo 1s to the p components in Mo 4d – Mo 5p hybridized orbitals, where the deviation from the perfect centrosymmetry (i.e. octahedral without distortion) governs the peak intensity.^[13] MoO₃ shows a modest pre-edge intensity (Figure 2b) reflecting the distorted octahedral symmetry of Mo atoms.

EXAFS Figure S4 shows the extended X-ray absorption fine structure (EXAFS) fit for the tetrahedral-dioxo structure and the pentahedral mono-oxo structure in catalysts with different loadings. The obtained bond lengths are 1.70–1.71 and 1.91–1.92 Å (Table S3). Minor contributions of pentahedral mono-oxo structures cannot be excluded, because the EXAFS fit for 2.1Mo assuming a pentahedral coordination, where the coordination numbers are constrained as $N = 1$ and $N = 4$, results in similar, however, less perfect agreement with the experimental spectrum (Figure S4A).

Table S3. Curve fit parameters for the single-scattering refinements^a of the EXAFS spectra of the dehydrated MoO_x/SBA-15 for the tetrahedral di-oxo (O=)₂Mo(–O–Si)₂ model (Figure S1). Uncertainties in the last significant digits are given in parentheses.

Sample	path	Assignment	N^b	R^c (Å)	σ^{2d} (Å ²)
2.1Mo	Mo–O	Mo=O	2	1.71(2)	0.0016(15)
	Mo–O	Mo–O–Si	2	1.92(3)	0.0014(18)
8.2Mo	Mo–O	Mo=O	2	1.70(2)	0.0005(12)
	Mo–O	Mo–O–Si	2	1.91(2)	0.0007(16)
13.3Mo	Mo–O	Mo=O	2	1.71(2)	0.0011(12)
	Mo–O	Mo–O–Si	2	1.92(3)	0.0019(19)

^a k range = 2–12 Å, R range = 1–2.09 Å, ^b coordination number, ^c distance, ^d EXAFS Debye-Waller factor.

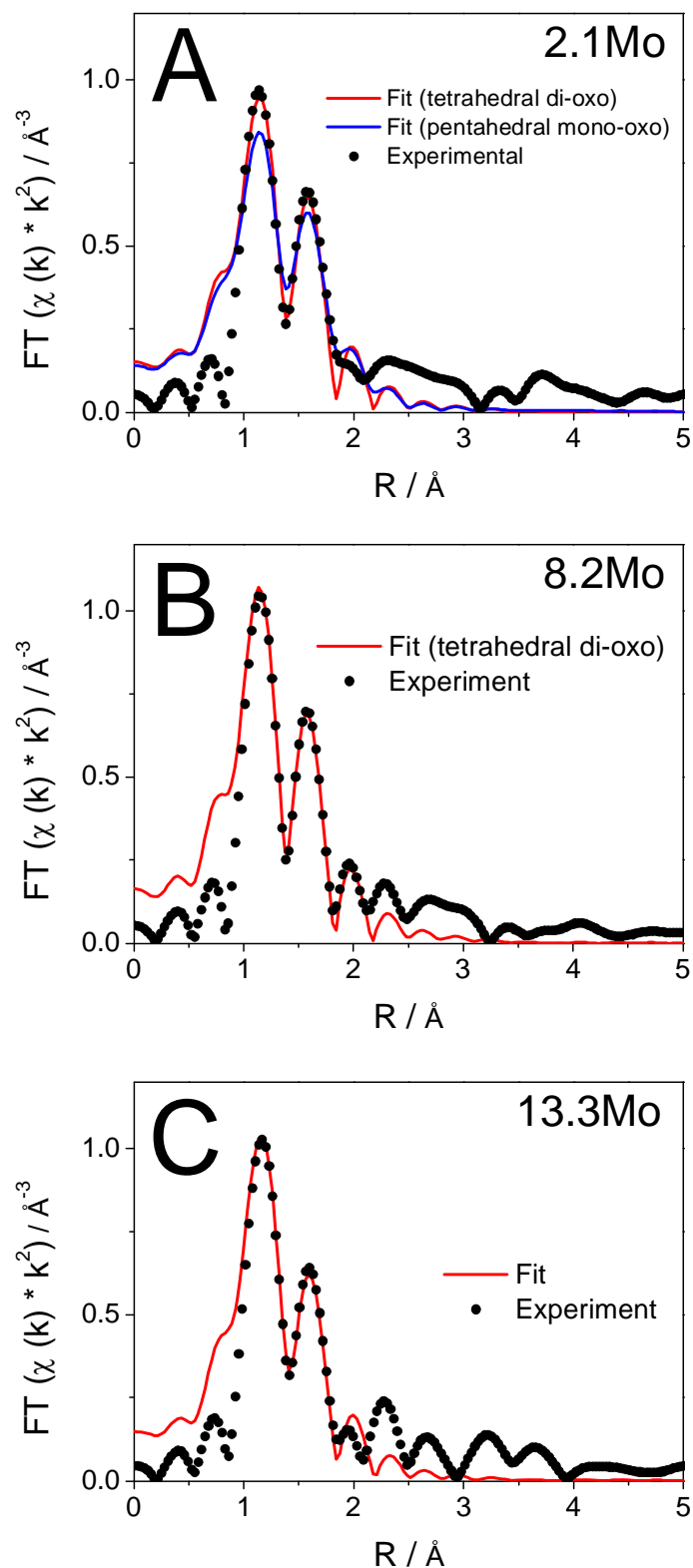


Figure S4. Magnitudes of Fourier-transformed k^2 -weighted Mo K-edge EXAFS spectra in non-phase-corrected R space for the dehydrated $\text{MoO}_x/\text{SBA-15}$ (dot) with curve fits to the single-scattering models for the tetrahedral-dioxo structure (red line) and the pentahedral mono-oxo structure (blue line, only for 2.1Mo): (A) 2.1Mo, (B) 8.2Mo, and (C) 13.3Mo. The fits were performed for the R range of 1~2.09 \AA .

3.3. O K-edge NEXAFS

Theoretical O 1s excitation spectra were calculated for cluster **a**–**c** (Figure S1). The calculated spectra of clusters **a** and **b** that possess isolated di-oxo MoO₄ structures anchored by 8-membered molybdosiloxane rings show a distinct double-peak structure, reproducing the experimental spectra of these low-loaded samples 2.1Mo, 5.1Mo and 6.6Mo (Figure S5A).

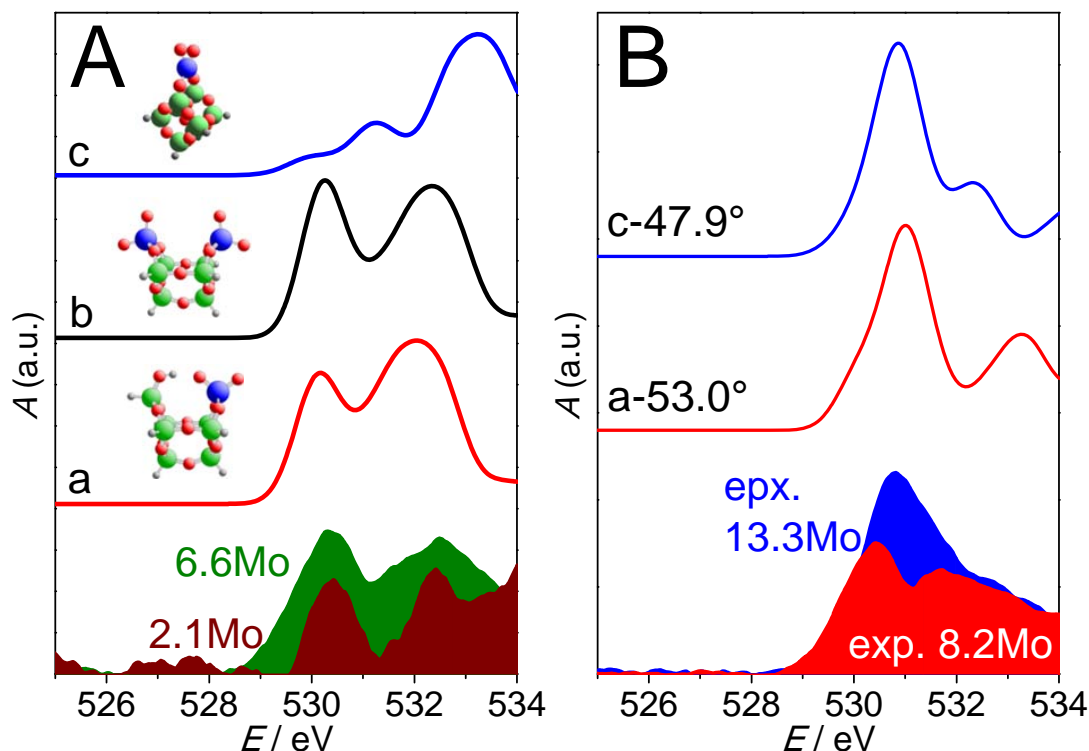


Figure S5. Theoretical and experimental O K-edge NEXAFS spectra. (A) Theoretical spectra for clusters **a**–**c** and experimental spectra of 2.1Mo and 6.6Mo. (B) Experimental spectra of 8.2Mo and 13.3Mo and theoretical spectra of modified cluster **a** and **c** where the O=Mo=O angle is changed to 53 and 47.9°, respectively. The spectra are arbitrary offset and scaled for clarity. Note that the absorption due to silica above 533 eV makes a large contribution in 2.1Mo due to the high Si/Mo ratio.

The theoretical O K-edge NEXAFS spectrum of cluster **c** (Figure S5A) is characterized by main absorption at 533.2 eV and weaker absorption at lower energy, which is totally different from any of the experimental spectra.

The structure of clusters **a** and **c** was modified by changing the O=Mo=O angle while freezing other geometric parameters. Figure S5B shows the experimental spectra of 8.2Mo and 13.3Mo and the theoretical spectra of angle-modified cluster **a** and **c** where the O=Mo=O angle is changed to 53 and 47.9°, respectively.

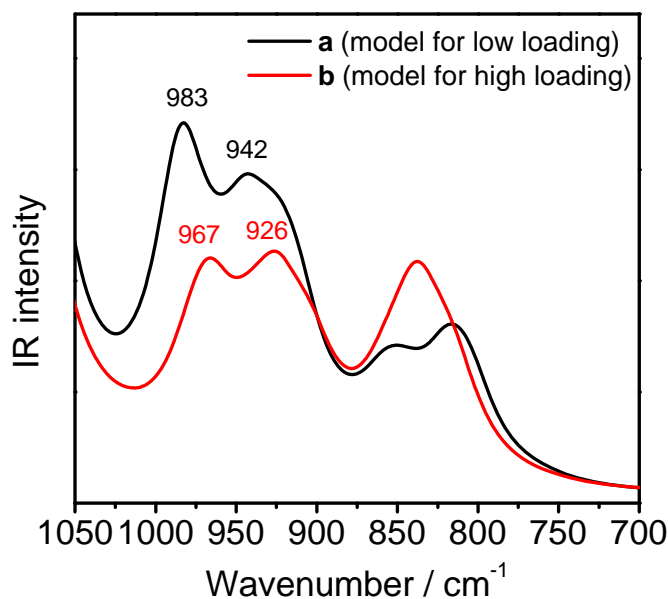


Figure S7. Calculated IR spectra for clusters **a** ($(\text{Si}-\text{O})_2\text{Mo}(=\text{O})_2$ with a $\text{Si}-\text{O}-\text{H}$ in the vicinity) and **b** (two adjacent $(\text{Si}-\text{O})_2\text{Mo}(=\text{O})_2$ units).

The calculated spectrum of cluster **b** (Figure S1) presents blue-shifted peak positions comparing to cluster **a** in the range between $900-1000\text{ cm}^{-1}$ (Figure S7), qualitatively reproducing the experimentally observed progressive blue shift along the increase of the molybdenum loading (Figure S6B and D).

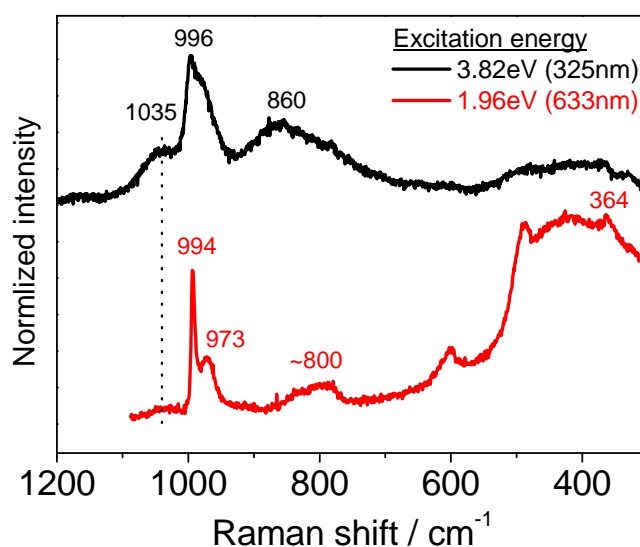


Figure S8. In situ Raman spectra of the dehydrated 8.2Mo measured at room temperature using excitation energies of 3.82 and 1.96 eV. The intensity was normalized at the $\text{Mo}=\text{O}$ band at $994-996\text{ cm}^{-1}$. The spectra were vertically offset for clarity.

Figure S8 displays Raman spectra of 8.2Mo upon two different excitation energies. The use of the near-resonant UV excitation results in the occurrence of new bands at 1035 and $\sim 860\text{ cm}^{-1}$. These bands are not due to silica.^[14] The band at 1035 cm^{-1} has been assigned to the stretching vibration of pentahedral mono-oxo $\text{O}=\text{Mo}(-\text{O}-\text{Si})_4$ species,^[15-18] suggesting that the pentahedral mono-oxo species in minor concentration show a

strong resonance enhancement at the excitation energy used (3.82 eV). The selective enhancement of pentahedral $\text{O}=\text{Mo}(\text{—O—Si})_4$ species over tetrahedral $(\text{Si—O—})_2\text{Mo}(=\text{O})_2$ species (bands at 994, 973 and 364 cm^{-1}) is reasonable, because the optical absorption edge energy of pentahedral species is generally higher than tetrahedral species.^[19] Among the spectroscopic methods used, only the UV Raman was able to detect pentahedral mono-oxo species, strongly indicating that the relative concentration of the mono-oxo species is rather low. This observation is indeed in agreement with the recent theoretical study by Handzlik and Ogonowski in which the authors showed that a minor fraction of the surface of amorphous silica prefers the formation of the mono-oxo species besides a predominant fraction of di-oxo species.^[18] The broad band at 860 cm^{-1} may be related to Mo—O—Si (as indicated in the theoretical spectra in Figure S7) or Mo—O—Mo stretch^[20] of minority polymeric species. The increased relative intensity of the band at $\sim 970 \text{ cm}^{-1}$ may be due to Mo—O—Si stretch of the mono-oxo species and/or the Si—OH vibration^[14] that is enhanced at this excitation condition.

4. Selectivity in Oxidative Dehydrogenation of Propane over $\text{MoO}_x/\text{SBA-15}$

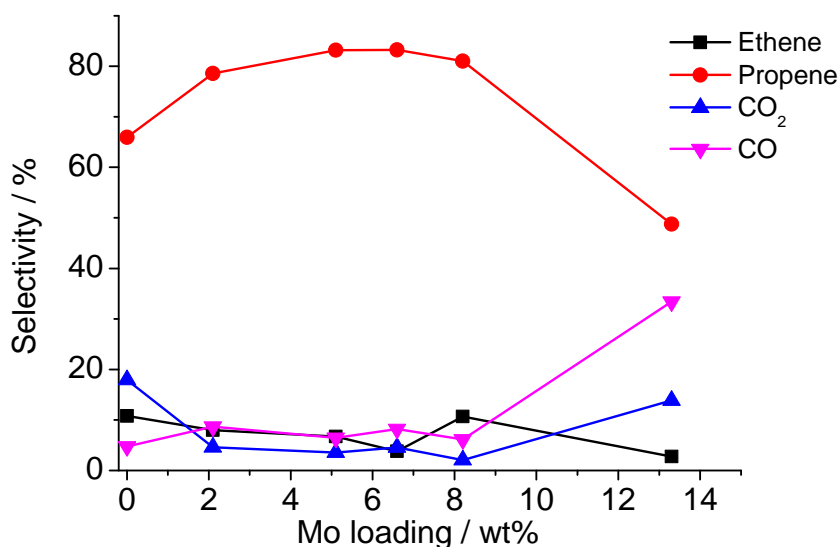


Figure S9. Selectivity in propane oxidation over $\text{MoO}_x/\text{SBA-15}$ catalysts. Reaction conditions: $T = 773\text{K}$, Feed; $\text{C}_3\text{H}_8/\text{O}_2/\text{N}_2=10/5/85$, contact time $0.6 \text{ s g}^{-1} \text{ ml}^{-1}$. Propane conversion was 0.11~0.63%.

References for Supporting Information

- [1] J. P. Thielemann, G. Weinberg, C. Hess, *ChemCatChem* **2011**, *3*, 1814–1821.
- [2] K. Amakawa, S. Wrabetz, J. Kröhnert, G. Tzolova-Müller, R. Schlögl, A. Trunschke, *J. Am. Chem. Soc.* **2012**, *134*, 11462–11473.
- [3] S. Ek, A. Root, M. Peussa, L. Niinistö, *Thermochim. Acta* **2001**, *379*, 201–212.
- [4] B. Ravel, M. Newville, *J. Synchrotron Rad.* **2005**, *12*, 537–541.
- [5] A. Knop-Gericke, E. Kleimenov, M. Hävecker, R. Blume, D. Teschner, S. Zafeirotos, R. Schlögl, V. I. Bukhtiyarov, V. V. Kaichev, I. P. Prosvirin, et al., *Adv. Catal.* **2009**, *52*, 213–272.
- [6] M. Hävecker, M. Cavalleri, R. Herbert, R. Follath, A. Knop-Gericke, C. Hess, K. Hermann, R. Schlögl, *Phys. Status Solidi B* **2009**, *246*, 1459–1469.
- [7] C. S. Guo, K. Hermann, M. Hävecker, J. P. Thielemann, P. Kube, L. J. Gregoriades, A. Trunschke, J. Sauer, R. Schlögl, *J. Phys. Chem. C* **2011**, *115*, 15449–15458.
- [8] K. Hermann, L. G. M. Pettersson, deMon developers group, *StoBe software V. 3.6, 2011*; see <http://www.fhi-berlin.mpg.de/KHsoftware/StoBe/>
- [9] G. Geudtner, P. Calaminici, J. Carmona-Espíndola, J. M. del Campo, V. D. Domínguez-Soria, R. F. Moreno, G. U. Gamboa, A. Goursot, A. M. Köster, J. U. Reveles, et al., *WIREs. Comput. Mol. Sci.* **2012**, *2*, 548–555.
- [10] G. Mestl, T. K. K. Srinivasan, *Catal. Rev. Sci. Technol.* **1998**, *40*, 451.
- [11] J. P. Baltrus, L. E. Makovsky, J. M. Stencel, D. M. Hercules, *Anal. Chem.* **1985**, *57*, 2500–2503.
- [12] N. Kakuta, K. Tohji, Y. Udagawa, *J. Phys. Chem.* **1988**, *92*, 2583–2587.
- [13] T. Yamamoto, *X-Ray Spectrom.* **2008**, *37*, 572–584.
- [14] F. L. Galeener, J. C. Mikkelsen, *Phys. Rev. B* **1981**, *23*, 5527–5530.
- [15] E. L. Lee, I. E. Wachs, *J. Phys. Chem. C* **2008**, *112*, 6487–6498.
- [16] E. L. Lee, I. E. Wachs, *J. Phys. Chem. C* **2007**, *111*, 14410–14425.
- [17] S. Chempath, Y. Zhang, A. T. Bell, *J. Phys. Chem. C* **2007**, *111*, 1291–1298.
- [18] J. Handzlik, J. Ogonowski, *J. Phys. Chem. C* **2012**, *116*, 5571–5584.
- [19] J. Jarupatrakorn, M. P. Coles, T. D. Tilley, *Chem. Mater.* **2005**, *17*, 1818–1828.
- [20] G. Xiong, C. Li, Z. Feng, P. Ying, Q. Xin, J. Liu, *J. Catal.* **1999**, *186*, 234–237.